A&A 630, L6 (2019)
https://doi.org/10.1051/0004-6361/201936277

Astronomy & Astrophysics

LETTER TO THE EDITOR

Mid-infrared evolution of η Carinae from 1968 to 2018*

A. Mehner[1], W.-J. de Wit[1], D. Asmus[2], P. W. Morris[3], C. Agliozzo[4], M. J. Barlow[5], T. R. Gull[6], D. J. Hillier[7], and G. Weigelt[8]

[1] ESO – European Organisation for Astronomical Research in the Southern Hemisphere, Alonso de Cordova 3107, Vitacura, Santiago de Chile, Chile
e-mail: amehner@eso.org
[2] Department of Physics & Astronomy, University of Southampton, Southampton SO17 1BJ, UK
[3] California Institute of Technology, IPAC, M/C 100-22, Pasadena, CA 91125, USA
[4] ESO – European Organisation for Astronomical Research in the Southern Hemisphere, Karl-Schwarzschild-Straße 2, 85748 Garching, Germany
[5] Department of Physics & Astronomy, University College London, Gower Street, London WC1E 6BT, UK
[6] NASA Goddard Space Flight Center, Code 667, Greenbelt, MD 20771, USA
[7] Department of Physics & Astronomy, University of Pittsburgh, 3941 O'Hara Street, Pittsburgh, PA 15260, USA
[8] Max Planck Institute for Radio Astronomy, Auf dem Hügel 69, 53121 Bonn, Germany

Received 9 July 2019 / Accepted 23 August 2019

ABSTRACT

η Car is one of the most luminous and massive stars in our Galaxy and is the brightest mid-IR source in the sky outside our solar system. Since the late 1990s, the central source has dramatically brightened at UV and optical wavelengths. This might be explained by a decrease in circumstellar dust extinction. We aim to establish the mid-IR flux evolution and further our understanding of the star's UV and optical brightening. Mid-IR images from 8−20 μm were obtained in 2018 with VISIR at the Very Large Telescope. Archival data from 2003 and 2005 were retrieved from the ESO Science Archive Facility, and historical records were collected from publications. We present mid-IR images of η Car with the highest angular resolution to date at the corresponding wavelengths (≥0.22″). We reconstruct the mid-IR evolution of the spectral energy distribution of the spatially integrated Homunculus nebula from 1968 to 2018 and find no long-term changes. The bolometric luminosity of η Car has been stable over the past five decades. We do not observe a long-term decrease in the mid-IR flux densities that could be associated with the brightening at UV and optical wavelengths, but circumstellar dust must be declining in our line of sight alone. Short-term flux variations within about 25% of the mean levels could be present.

Key words. circumstellar matter – stars: individual: η Car – stars: massive – stars: mass-loss – stars: variables: S Doradus – stars: winds, outflows

1. Introduction

η Car is the archetype of unstable massive stars, eruptive mass loss, and supernova (SN) impostors, and it is a reference for understanding the precursor eruptions that lead to superluminous SNe. The star has a current mass of about 100 $M_\odot$ and is in an eccentric binary system (Damineli et al. 1997; Davidson & Humphreys 2012 and references therein). During an eruptive event in the nineteenth century (see Frew 2004 for the historical lightcurve), the system ejected ≥45 $M_\odot$ of material (Morris et al. 2017; see also Smith et al. 2003) that forms the bipolar Homunculus nebula.

η Car is often as an extreme case of a luminous blue variable (LBV). LBVs are evolved massive stars with initial masses ≥20 $M_\odot$ that exhibit instabilities that are not understood, resulting in enhanced mass loss (Conti 1984, 1997; Humphreys & Davidson 1994; Nota & Lamers 1997). They have been considered to be stars in transition to the Wolf-Rayet stage (e.g., Maeder 1983; Langer et al. 1994), but more recent observational and theoretical work suggests that some LBVs might be the immediate progenitors of SNe (e.g., Kotak & Vink 2006; Trundle et al. 2008; Gal-Yam & Leonard 2009; Smith et al. 2007; Groh et al. 2013).

A crucial parameter for understanding η Car is the luminosity because this provides a mass estimate through the Eddington limit. Most of the visible and UV light of η Car is absorbed by circumstellar dust and is reradiated in the IR (Davidson 1971; Davidson & Ostriker 1972; Pagel 1969; Westphal & Neugebauer 1969; Robinson et al. 1973; Sutton et al. 1974). The stellar luminosity can thus be obtained from the IR spectral energy distribution (SED). η Car is unparalleled as an IR radiation source, and its brightness makes observations with sensitive IR satellite instrumentation impossible. Most of the 0.25−0.44 $M_\odot$ of cool dust is located in the central 5″ region in a "disrupted" equatorial structure (Morris et al. 1999, 2017) that is also referred to as the Butterfly nebula (Chesneau et al. 2005). Early estimates of the total luminosity of η Car are on the order of $L = 5 \times 10^6\ L_\odot$ (Neugebauer & Westphal 1968; Westphal & Neugebauer 1969; Pagel 1969; Robinson et al. 1973; Sutton et al. 1974; Cox et al. 1995; Davidson & Humphreys 1997). Morris et al. (2017)

* Based on observations collected at ESO's Very Large Telescope under Prog-IDs: 074.A-9016(A), 0101.D-0077(A). Based on observations made with ESO Telescopes at the La Silla Paranal Observatory under Prog-IDs: 60.A-9126(A,C,E,I), 69.D-0304(B),71.D-0049(A).

concluded that the total luminosity of η Car in the 1970s was $L = 4.1 \times 10^6\,L_\odot$ for the commonly adopted distance of 2.3 kpc. A distance revision to 2.6 kpc could imply an increase in luminosity of 25–30% (Davidson et al. 2018a). The luminosity of the secondary star is a factor of 10 lower (Mehner et al. 2010).

Some authors have suggested a change in the mid-IR flux since the 1970s. Russell et al. (1987) reported a 30% decrease in the 10.5 μm silicate emission compared to values for the 1970s. Smith et al. (1995) found a significant decrease in mid-IR flux in the 1990s compared to the 1970s. Morris et al. (2017) derived a total luminosity of $L = 3.0 \times 10^6\,L_\odot$ for the 1990s, which is a decline of 25% in 20 yr. They argued that the decline in mid-IR flux indicates a reduction in circumstellar extinction either by the expansion of dust shells or dust destruction. This could cause the simultaneous brightening at UV and optical wavelengths (Davidson et al. 1999, 2005; Martin et al. 2006).

We present newly obtained and previously unpublished mid-IR observations, which are the basis of a reevaluation of the mid-IR evolution of η Car from 1968 to 2018. In Sect. 2 we describe the new mid-IR images. We present our findings and reanalyze the SED of η Car over a period of 50 years in Sect. 3. In Sect. 4 we conclude that η Car has not undergone any appreciable long-term luminosity changes during this period.

2. Mid-IR observations in 2005 and 2018 with VISIR and in 2003 with TIMMI2

η Car was observed in 2018 with the upgraded VLT imager and spectrometer for the mid-IR (VISIR; Lagage et al. 2004; Käufl et al. 2015). The VISIR AQUARIUS detector provides a field of view of 38.0″ × 38.0″ with a pixel scale of 0.045″. We sampled the mid-IR wavelength range with several filters from 7.8–19.5 μm, see Tables 1 and B.1, and Fig. A.1. The observations were carried out at an airmass below 1.3 and at a precipitable water vapor between 1.2 and 3.5 mm, ensuring good image quality. The burst read-out mode was used, which results in a large number of short-exposure images with instantaneous point spread functions, corresponding to the momentary atmospheric turbulence. High spatial resolution images can be obtained by recentering and adding the individual short-exposure images. We reach spatial resolutions close to the diffraction limits in the given filters: 0.25–0.30″ in N band and ~0.50″ in Q band. For the flux calibration, the science observations were either preceded or followed by observations of a mid-IR standard star (HD89682; Cohen et al. 1999) that were obtained with the same setup as the science observations.

The data reduction was performed with a custom-made PYTHON pipeline. The photometry was determined using classical aperture photometry with an aperture radius of 11″, which encompasses the entire Homunculus nebula. VISIR absolute flux calibration is accurate to 10% in the N band and 20% in the Q band. The dominating source of uncertainty is the mid-IR sky variability. The count levels in the central bright core of the Homunculus nebula (1″ in diameter, see Fig. 1) are outside the linear regime for most filters, which implies that we may be underestimating the total flux by a few percent. We did not attempt to correct for this because longward of 8 μm less than 10% and longward of 10 μm less than 5% of the flux is produced by this central core. The resulting mid-IR spectral flux densities and statistical uncertainties are listed in Table 1.

In what follows, we reconstruct the mid-IR SED with our 2018 observations and literature data (references are provided in the caption of Fig. 2). In order to be as complete as possible, we also make use of mid-IR images in the ESO Science Archive Facility with unpublished photometry[1]. η Car was observed with VISIR in 2005 in the filters PAH1, PAH2, NeII, and Q2 with the former Boeing detector. Standard star observations were only obtained in the filters PAH2 and NeII, see Table B.1. The pixel scale is 0.075″ and the images have spatial resolutions of ~0.35″. Detector artifacts, such as strong striping and ghosts, result in poor flux measurements. In January, March, and May 2003, η Car was observed with the Thermal infrared Multi-Mode instrument (TIMMI2, Reimann et al. 2000) at the La Silla 3.6 m telescope, see Table B.2. The TIMMI2 array shows smear and stripe patterns for bright sources, which lead to large errors in the flux calibration. We have averaged the flux values of all TIMMI2 observations and present the standard deviation as errors in Table 1. The TIMMI2 data should be interpreted with caution.

Table 1. Mid-IR flux densities of the spatially integrated Homunculus nebula (2003–2018) around η Car.

Filter	Wavelength (μm)	Date	Flux density (Jy)	Error flux density [a] (Jy)
		VISIR		
J7.9	7.78	2018-05-21	9648	30
PAH1	8.59	2018-04-28	19 280	40
ArIII	8.99	2018-12-10	31 140	80
SIV_1	9.82	2018-05-21	51 030	220
SIV	10.49	2018-04-29	54 520	160
PAH2	11.25	2018-12-10	66 660	210
B12.4	12.47	2018-04-29	53 930	230
NeII	12.81	2018-12-10	63 120	470
NeII_2	13.04	2018-12-10	58 410	450
Q1	17.65	2018-05-11	93 040	2690
Q2	18.72	2018-05-11	100 810	3550
Q3	19.50	2018-05-11	97 380	9940
PAH2	11.25	2005-01-23	61 350	390
NeII [b]	12.81	2005-01-23	44 420	1050
		TIMMI2 [c]		
M	4.6	2003	3590	1230
N7.9	7.9	2003	13 260	3880
N8.9	8.7	2003	23 650	7810
N9.8	9.6	2003	40 590	2840
N10.4	10.3	2003	47 710	5060
N11.9	11.6	2003	63 360	6980
N12.9	12.3	2003	60 000	6100
[NeII]	12.8	2003	80 960	8170
Q1	17.8	2003	122 190	15 190

Notes. [a]Formal errors from the flux calibration. Systematic uncertainties due to sky variability and detector artifacts can be larger than 10% for N band and 20% for Q band. [b]Observations are strongly affected by ghosts. [c]Average of observations in January, March, and May 2003. The data are badly affected by stripe patterns.

3. Results

3.1. Flux evolution in the mid-IR

Figure 2 compares the 2018 mid-IR photometry from our VISIR images with previous observations in the period 1968–2005.

[1] http://archive.eso.org

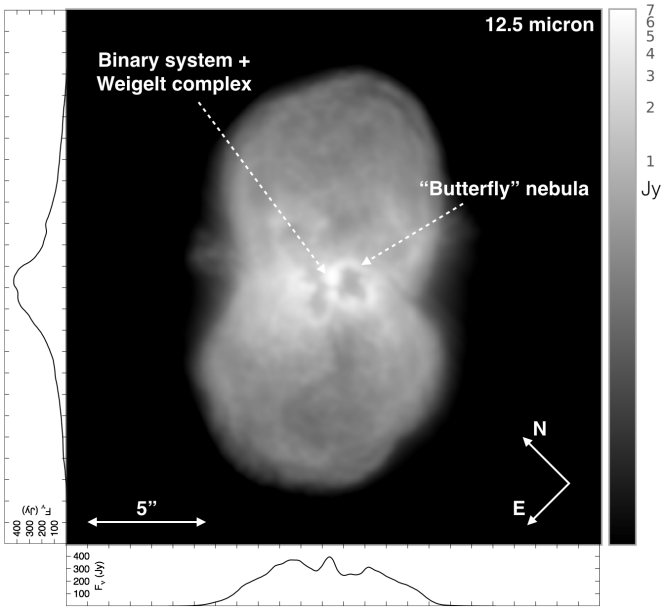

Fig. 1. VISIR image of the Homunculus nebula at 12.5 μm in 2018, tracing the thermal emission from heated dust and the H I 7−6 emission. The field of view is 25″ × 25″, and the spatial resolution is 0.3″. The flux density in Jy per detector pixel (0.045″ pixel^{-1}) is shown as well as the integrated flux along the image axes. The brightest knot in the center of the nebula is due to a shell that surrounds the star, to an inner torus or disk, or to a pin-wheel structure, and it includes the Weigelt complex (Weigelt & Ebersberger 1986). The two bright loops form the Butterfly nebula from which 50% of the integrated flux originates.

Figure 3 displays the time evolution of four mid-IR wavelength regions over 50 years and their averages. With a few exceptions, individual values are consistent with each other within 1σ (22% for M band, 13% for N band, and 19% for Q band) of the average. The figures demonstrate long-term stability of the mid-IR flux between 5 and 20 μm over 50 years within the uncertainty of mid-IR flux calibration.

The timescales for the condensation and destruction of dust grains depend on the chemistry and shielding conditions, which are complex in the Homunculus nebula around η Car. Ionizing UV and X-ray radiation that escapes from the central binary varies with orbital phase, but we cannot confirm periodic changes in the mid-IR because the observations were obtained at a mix of orbital phases, the orbital coverage is sparse, and the calibration uncertainties are large. The observations in 1971/72 indicate a trend to higher flux values in mid-cycle, similar to what is observed in the radio (White et al. 2005), but Robinson et al. (1973) stated that there is no evidence for variations from October 1971 to July 1972 larger than the measurement uncertainties. Polomski et al. (1999) found that the N band and 18 μm flux density increased between March 1997 and November 1998, that is, around periastron. The emission of the central bright core (1″ in diameter) contributes to less than 10% at 8 μm, 5% at 10 μm, 4% at 13 μm, and 2% at 19 μm. Any variations due to recent dust formation or destruction close to the star is hidden in the uncertainties of the nebula-encompassing photometry.

Morris et al. (2017) reported that the mid-IR flux of η Car decreased by 25% over the past decades[2]. Their result was based on data obtained in 1996 with the spectrometers on board the Infrared Space Observatory (ISO; Kessler et al. 1996). While the absolute spectrophotometric calibration of the ISO spectra was hampered by different detector materials with their own signal-dependent susceptibilities to nonlinearities and memory effects (e.g., Van Malderen et al. 2004; Morris et al. 2017), the reported decline may at least partly be due to intrinsic orbital variations. A detailed color-temperature analysis with orbital phase will reveal the thermal characteristics of short-term variations, but such a study will require a more homogeneous set of spatial and temporal monitoring observations.

In contrast to Russell et al. (1987), Smith et al. (1995), and Morris et al. (2017), our SED re-construction and investigation of the time evolution does not reveal a noticeable long-term decrease in the mid-IR flux from 8 to 20 μm since the first available mid-IR photometry in the late 1960s (see Figs. 2 and 3). The data support a rather stable mid-IR flux over 50 years, within the large uncertainties of ground-based mid-IR photometry and excluding variations within ~25% of the mean levels. As a consequence, the UV and optical brightening since the late 1990s does not correlate with the integrated mid-IR flux. This is an important finding because the lack of any systematic mid-IR flux change rules out large changes in the luminosity of η Car. We derive a luminosity of about $4.6 \times 10^6\,L_\odot$ for η Car, using the 2.3 μm, 3.4 μm, and 4.9 μm photometry of Gehrz et al. (1973), the 2005 and 2018 VISIR mid-IR photometry, and the flux values at 35−175 μm by Harvey et al. (1978) and at 450 μm and 850 μm by Gomez et al. (2010).

3.2. Dust extinction

Ever since the 1940s, η Car has brightened steadily at optical wavelengths (Frew 2004), and an accelerated brightening has been observed since the late 1990s (Davidson et al. 1999). Today, η Car at UV and visual wavelengths is more than 2 mag brighter than in the 1990s and the change is remarkably gray (Davidson et al. 2018b; Damineli et al. 2019). Because η Car is close to the Eddington limit, this can in principle not constitute an increase in bolometric luminosity. Davidson et al. (1999, 2005) and Martin et al. (2006) attributed this brightening to a rapid decrease in circumstellar extinction. The material around η Car is not distributed spherically. The central region is seen through a dust condensation, which strongly attenuates the central source (Hillier & Allen 1992; Weigelt et al. 1995). Davidson et al. (1999) argue that movement of a dusty condensation that intercepts our line-of-sight is unlikely, leaving dust destruction or a decrease of the dust formation rate close to the star as possible explanations. A possible cause may also be small changes in the stellar parameters, which alter the shape of the wind-wind shock cone such that we no longer look through the newly formed dust. Damineli et al. (2019) proposed the dissipation of a dusty clump ("coronagraph") in our line of sight.

The variability in the near-IR from 1972 to 2013 was studied by Whitelock et al. (2004) and Mehner et al. (2014). The star shows a long-term brightening in JHK, whereas the L-band emission remains basically constant. The 4−8 μm flux shows no long-term variation either (Russell et al. 1987; Fig. 3). Because longward of 4 μm thermal radiation dominates the SED rather than extinction, we would expect a significant decrease in flux in the 10−20 μm range only for a net destruction of warm (~200 K) dust grains. Nonetheless, Fig. 3 indicates a short-term increase in

[2] The values displayed in Fig. 7 in Morris et al. (2017) are too high for the 11 μm photometry by Gehrz et al. (1973) because of a transcription error. The flux values at 11 μm reported in Table 1 and Fig. 1 of Gehrz et al. (1973) are inconsistent by a factor of about 2. We use the values from their Table 1.

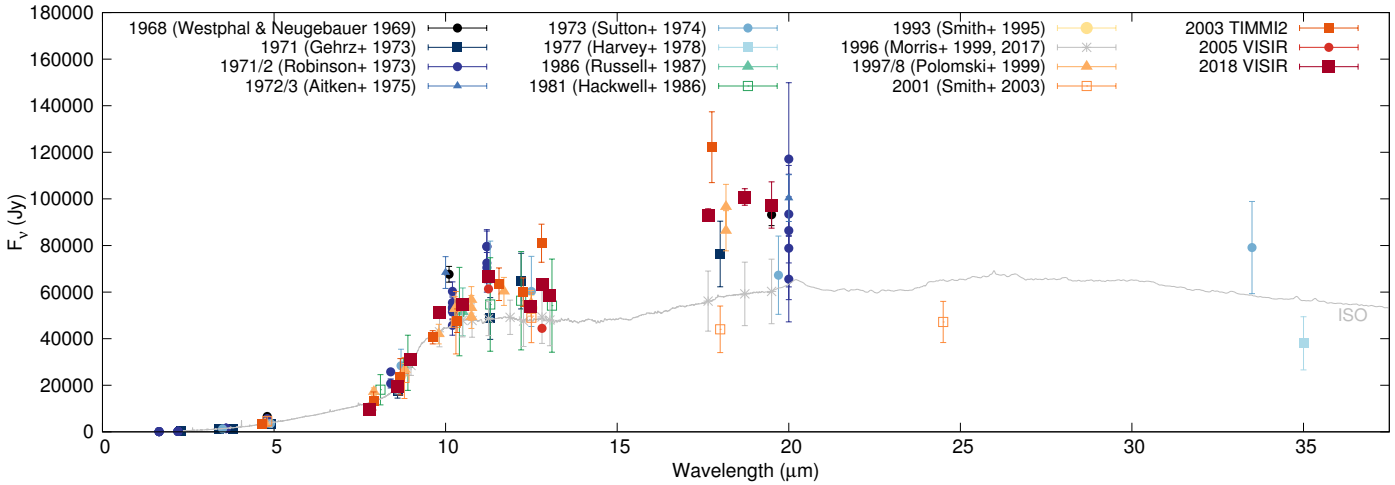

Fig. 2. Mid-IR photometry of the integrated Homunculus nebula from 1968 to 2018. Colored symbols represent our new and historic mid-IR measurements performed in the 1960s (Westphal & Neugebauer 1969), 1970s (Gehrz et al. 1973; Robinson et al. 1973; Aitken & Jones 1975; Sutton et al. 1974; Harvey et al. 1978), 1980s (Hackwell et al. 1986; Russell et al. 1987), 1990s (Smith et al. 1995; Polomski et al. 1999; Morris et al. 1999, 2017), and 2000s (Smith et al. 2003). Calibration uncertainties may be larger than reported because of unaccounted for systematic uncertainties, sky variability, detector artifacts, and partial saturation. Open symbols represent values estimated from isophotal contour maps (Hackwell et al. 1986; Smith et al. 2003).

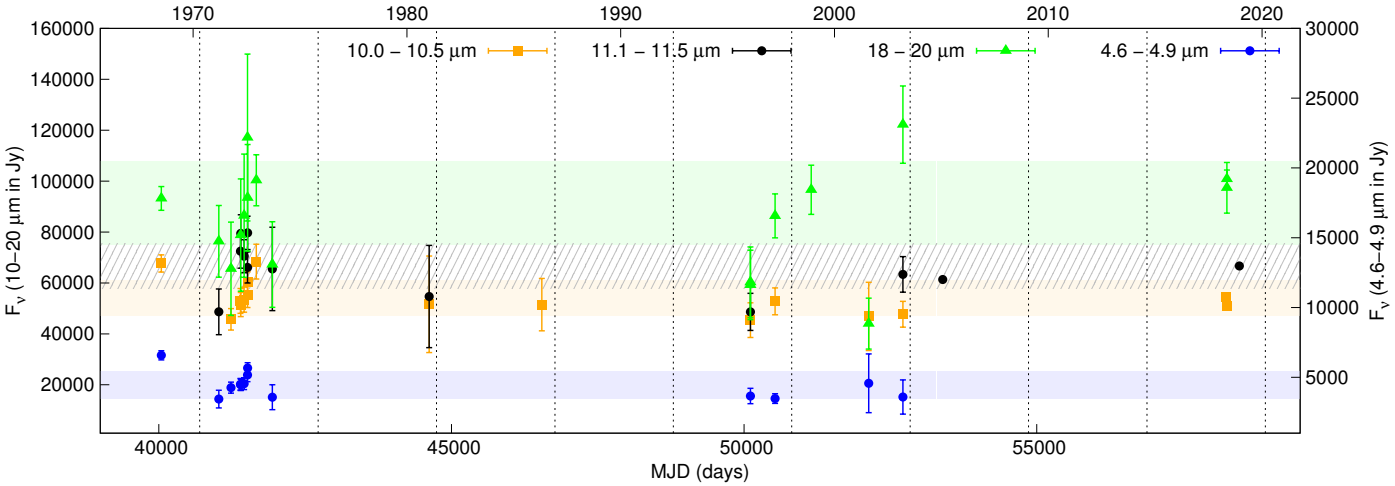

Fig. 3. Time evolution of the mid-IR flux of the Homunculus nebula around η Car from 1968 to 2018 in four wavelength regions, chosen for best temporal coverage. Vertical dashed lines indicate periastron passages. The 1σ region of the average flux for each wavelength region is shown (averages exclude the lower ISO flux values). There is no evidence for a long-term change, but variations with the orbital period cannot be ruled out.

emission levels at mid-cycle in the 1970s and during periastron in 1998.

The extinction of the UV and optical light is probably caused predominantly by dust within the inner core. In the VISIR J7.9 filter image, the central core is resolved in at least three knots (Fig. A.1). In the PAH2 and NeII filters, for which we have comparison VISIR images in 2005, this core is unresolved. For an aperture of 0.5″ radius around the central bright source, we derive $F_{\nu,\,\mathrm{PAH2},\,2005} = 3130 \pm 50$ Jy and $F_{\nu,\,\mathrm{NeII},\,2005} = 2710 \pm 180$ Jy, compared with $F_{\nu,\,\mathrm{PAH2},\,2018} = 3140 \pm 10$ Jy and $F_{\nu,\,\mathrm{NeII},\,2018} = 3200 \pm 30$ Jy. Additional systematic errors are about 10%. There appears to be no detectable change in mid-IR flux of the inner core in the last 13 yr. This implies either an equilibrium or very weak dust formation and destruction close to the star. If the geometry of this central knot would simply expand, then the optical depth τ(UV, optical) would decline, depending on grain properties (chemistry, shape, and size). In this case, and if τ(IR) < 1, we would expect a small effect (<2−10% depending on wavelength and hidden in the uncertainties) in the integrated mid-IR flux because the IR emission is determined by the larger nebula. Any stochastic increase or decrease in line-of-sight dust instantly changes the UV and optical extinction but not the IR emission because the dust particles are heated and will radiate.

3.3. Resolved dusty circumstellar structures

Several authors have suggested a disk-, ring-, or torus-like structure of 5−6″ in diameter around the central star, which absorbs, scatters, and reradiates the stellar radiation in the IR (Gehrz et al. 1973; Sutton et al. 1974; Hyland et al. 1979; Warren-Smith et al. 1978; Rigaut & Gehring 1995; Smith et al. 1995; Polomski et al. 1999). Morris et al. (1999) showed that most of the dust in the equatorial region is located in toroidal structures, probably

created in shock-heated gas of the nineteenth century eruption. Some dust may also be located in an inner unresolved torus or disk and/or pinwheel-like structures created by colliding winds in the orbital plane (Weigelt et al. 2016). Smith et al. (2002) presented mid-IR images from 4.8 to 24.5 μm that support the hypothesis of a circumstellar torus or disk. Artigau et al. (2011) argued that this Butterfly nebula (Chesneau et al. 2005) is not a coherent physical structure or equatorial torus, but consists of spatially separate clumps and filaments that were ejected at different times. Radial velocity information from ALMA observations supports the general picture that the loops are a pinched torus in the orbital plane, perpendicular to the Homunculus lobes (Smith et al. 2018). The direction of the pinched material matches periastron/apastron orientation (Madura et al. 2013) and the companion may have played a role in disrupting the torus soon after its ejection.

The geometry of the dust surrounding η Car is quite complex, see Fig. 1 (also Smith et al. 2002). In the center, two bright ring-like structures form the Butterfly nebula. Most of the dust is located in this central region (50% of the flux originates within a 3″ radius from the central source, and 80% within a 5″ radius). In the mid-IR, we can identify strong density or temperature gradients and knots along these loops, but also spatially coherent structures.

Comparison between the 2005 and 2018 VISIR images show that the two prominent loops are expanding at a rate of up to 0.01″ yr^{-1} projected on sky. This corresponds to projected velocities of ~100 km s^{-1} at a distance of 2.3 kpc, which is consistent with velocities in the equatorial plane (Davidson et al. 2001). The rings seem to expand without losing their overall appearance, which supports the idea that these are physically coherent structures. The farthest extent of the Butterfly nebula is about 2″ from the central source, which points toward an ejection during or in the decades before the nineteenth century eruption. We do not find any brightness changes of the inner loop-like structures between observations separated by 13 years. For an aperture of 3″ radius, we derive $F_{\nu,\,\mathrm{PAH2},\,2005} = 34170 \pm 520$ Jy and $F_{\nu,\,\mathrm{NeII},\,2005} = 30100 \pm 2010$ Jy, compared with $F_{\nu,\,\mathrm{PAH2},\,2018} = 34500 \pm 150$ Jy and $F_{\nu,\,\mathrm{NeII},\,2018} = 32020 \pm 280$ Jy. The response time for the dust formation or destruction at these distances from the star is not clear. However, the constant flux and overall appearance of these loops may imply that there is no recent dust formation or destruction and the material is simply expanding because these structures are likely optically thin.

Clues to the history and origin of mass ejection phases of η Car can be found in its circumstellar material. Hydrodynamical simulations show that a spherical mass ejection into a massive pre-existing torus of gas and dust could result in the present-day bipolar geometry of the Homunculus nebula (Frank et al. 1995; Dwarkadas & Balick 1998). The massive torus may have been created shortly before the nineteenth century eruption, for instance, through nonconservative mass transfer, leaving an unstable core that then erupted.

4. Conclusions

The mid-IR flux densities of the Homunculus nebula around η Car from 8 to 20 μm show no long-term decline since the first available mid-IR photometry in 1968. The luminosity of η Car has thus probably been stable over the past five decades (~$4.6 \times 10^6\,L_\odot$, adopting a distance of 2.3 kpc). Mid-IR observations were obtained irregularly and at different orbital phases. The large uncertainties of the mid-IR photometry (10% in N band and 20% in Q band) prevents the confirmation of smaller short-term fluctuations or variations with the orbital period.

Contrary to previous publications, we find no long-term decline of the mid-IR photometric levels, which would have indicated a reduction in circumstellar extinction and could have explained the increase in UV and optical brightness. The most likely scenario to explain the brightening of η Car at UV and optical wavelengths and its stability in the mid-IR is that the extinction caused by circumstellar dust declines only in our line of sight.

Acknowledgements. We thank the anonymous referee for the constructive feedback. MJB acknowledges support from ERC grant SNDUST 694520. We have used SketchAndCalc to calculate the areas in isophotal contour maps (E. M. Dobbs; `www.SketchAndCalc.com`).

References

Aitken, D. K., & Jones, B. 1975, MNRAS, 172, 141
Artigau, É., Martin, J. C., Humphreys, R. M., et al. 2011, AJ, 141, 202
Chesneau, O., Min, M., Herbst, T., et al. 2005, A&A, 435, 1043
Cohen, M., Walker, R. G., Carter, B., et al. 1999, AJ, 117, 1864
Conti, P. S. 1984, in Observational Tests of the Stellar Evolution Theory, eds. A. Maeder, & A. Renzini, IAU Symp., 105, 233
Conti, P. S. 1997, in Luminous Blue Variables: Massive Stars in Transition, eds. A. Nota, & H. Lamers, ASP Conf. Ser., 120, 387
Cox, P., Mezger, P. G., Sievers, A., et al. 1995, A&A, 297, 168
Damineli, A., Conti, P. S., & Lopes, D. F. 1997, New Astron., 2, 107
Damineli, A., Fernández-Lajús, E., Almeida, L. A., et al. 2019, MNRAS, 484, 1325
Davidson, K. 1971, MNRAS, 154, 415
Davidson, K., & Humphreys, R. M. 1997, ARA&A, 35, 1
Davidson, K., & Humphreys, R. M. 2012, in Eta Carinae and the Supernova Impostors, Astron. Space Sci. Lib., 384
Davidson, K., & Ostriker, J. P. 1972, Nat. Phys. Sci., 236, 46
Davidson, K., Gull, T. R., Humphreys, R. M., et al. 1999, AJ, 118, 1777
Davidson, K., Smith, N., Gull, T. R., Ishibashi, K., & Hillier, D. J. 2001, AJ, 121, 1569
Davidson, K., Martin, J., Humphreys, R. M., et al. 2005, AJ, 129, 900
Davidson, K., Helmel, G., & Humphreys, R. M. 2018a, Res. Notes AAS, 2, 133
Davidson, K., Ishibashi, K., Martin, J. C., & Humphreys, R. M. 2018b, ApJ, 858, 109
Dwarkadas, V. V., & Balick, B. 1998, AJ, 116, 829
Frank, A., Balick, B., & Davidson, K. 1995, ApJ, 441, L77
Frew, D. J. 2004, J. Astron. Data, 10, 6
Gal-Yam, A., & Leonard, D. C. 2009, Nature, 458, 865
Gehrz, R. D., Ney, E. P., Becklin, E. E., & Neugebauer, G. 1973, Astrophys. Lett., 13, 89
Gomez, H. L., Vlahakis, C., Stretch, C. M., et al. 2010, MNRAS, 401, L48
Groh, J. H., Meynet, G., & Ekström, S. 2013, A&A, 550, L7
Hackwell, J. A., Gehrz, R. D., & Grasdalen, G. L. 1986, ApJ, 311, 380
Harvey, P. M., Hoffmann, W. F., & Campbell, M. F. 1978, A&A, 70, 165
Hillier, D. J., & Allen, D. A. 1992, A&A, 262, 153
Humphreys, R. M., & Davidson, K. 1994, PASP, 106, 1025
Hyland, A. R., Robinson, G., Mitchell, R. M., Thomas, J. A., & Becklin, E. E. 1979, ApJ, 233, 145
Käufl, H. U., Kerber, F., Asmus, D., et al. 2015, The Messenger, 159, 15
Kessler, M. F., Steinz, J. A., Anderegg, M. E., et al. 1996, A&A, 315, L27
Kotak, R., & Vink, J. S. 2006, A&A, 460, L5
Lagage, P. O., Pel, J. W., Authier, M., et al. 2004, The Messenger, 117, 12
Langer, N., Hamann, W.-R., Lennon, M., et al. 1994, A&A, 290, 819
Madura, T. I., Gull, T. R., Okazaki, A. T., et al. 2013, MNRAS, 436, 3820
Maeder, A. 1983, A&A, 120, 113
Martin, J. C., Davidson, K., & Koppelman, M. D. 2006, AJ, 132, 2717
Mehner, A., Davidson, K., Ferland, G. J., & Humphreys, R. M. 2010, ApJ, 710, 729
Mehner, A., Ishibashi, K., Whitelock, P., et al. 2014, A&A, 564, A14
Morris, P. W., Waters, L. B. F. M., Barlow, M. J., et al. 1999, Nature, 402, 502
Morris, P. W., Gull, T. R., Hillier, D. J., et al. 2017, ApJ, 842, 79
Neugebauer, G., & Westphal, J. A. 1968, ApJ, 152, L89

Nota, A., & Lamers, H. 1997, in Luminous Blue Variables: Massive Stars in Transition, ASP Conf. Ser., 120
Pagel, B. E. T. 1969, Astrophys. Lett., 4, 221
Polomski, E. F., Telesco, C. M., Piña, R. K., & Fisher, R. S. 1999, AJ, 118, 2369
Reimann, H. G., Linz, H., Wagner, R., et al. 2000, in Optical and IR Telescope Instrumentation and Detectors, eds. M. Iye, & A. F. Moorwood, Proc. SPIE, 4008, 1132
Rigaut, F., & Gehring, G. 1995, in Revista Mexicana de Astronomia y Astrofisica, Ser. Conf., eds. V. Niemela, N. Morrell, & A. Feinstein, 2, 27
Robinson, G., Hyland, A. R., & Thomas, J. A. 1973, MNRAS, 161, 281
Russell, R. W., Lynch, D. K., Hackwell, J. A., et al. 1987, ApJ, 321, 937
Smith, C. H., Aitken, D. K., Moore, T. J. T., et al. 1995, MNRAS, 273, 354
Smith, N., Gehrz, R. D., Hinz, P. M., et al. 2002, ApJ, 567, L77
Smith, N., Gehrz, R. D., Hinz, P. M., et al. 2003, AJ, 125, 1458
Smith, N., Li, W., Foley, R. J., et al. 2007, ApJ, 666, 1116
Smith, N., Ginsburg, A., & Bally, J. 2018, MNRAS, 474, 4988
Sutton, E., Becklin, E. E., & Neugebauer, G. 1974, ApJ, 190, L69
Trundle, C., Kotak, R., Vink, J. S., & Meikle, W. P. S. 2008, A&A, 483, L47
Van Malderen, R., Decin, L., Kester, D., et al. 2004, A&A, 414, 677
Warren-Smith, R. F., Scarrot, S. M., Murdin, P., & Bingham, R. G. 1978, Mem. Soc. Astron. It., 49, 589
Weigelt, G., & Ebersberger, J. 1986, A&A, 163, L5
Weigelt, G., Albrecht, R., Barbieri, C., et al. 1995, in The Eta Carinae Region: A laboratory of Stellar Evolution, La Plata Argentina, Nov 22–26, 1993, eds. V. Niemela, N. Morrell, & A. Feinstein, Revista Mexicana de Astronomia y Astrofisica Serie de Conferencias, 2, 11
Weigelt, G., Hofmann, K.-H., Schertl, D., et al. 2016, A&A, 594, A106
Westphal, J. A., & Neugebauer, G. 1969, ApJ, 156, L45
White, S. M., Duncan, R. A., Chapman, J. M., & Koribalski, B. 2005, in The Fate of the Most Massive Stars, eds. R. Humphreys, & K. Stanek, ASP Conf. Ser., 332, 129
Whitelock, P. A., Feast, M. W., Marang, F., & Breedt, E. 2004, MNRAS, 352, 447

Appendix A: Mid-IR images with VISIR in 2018

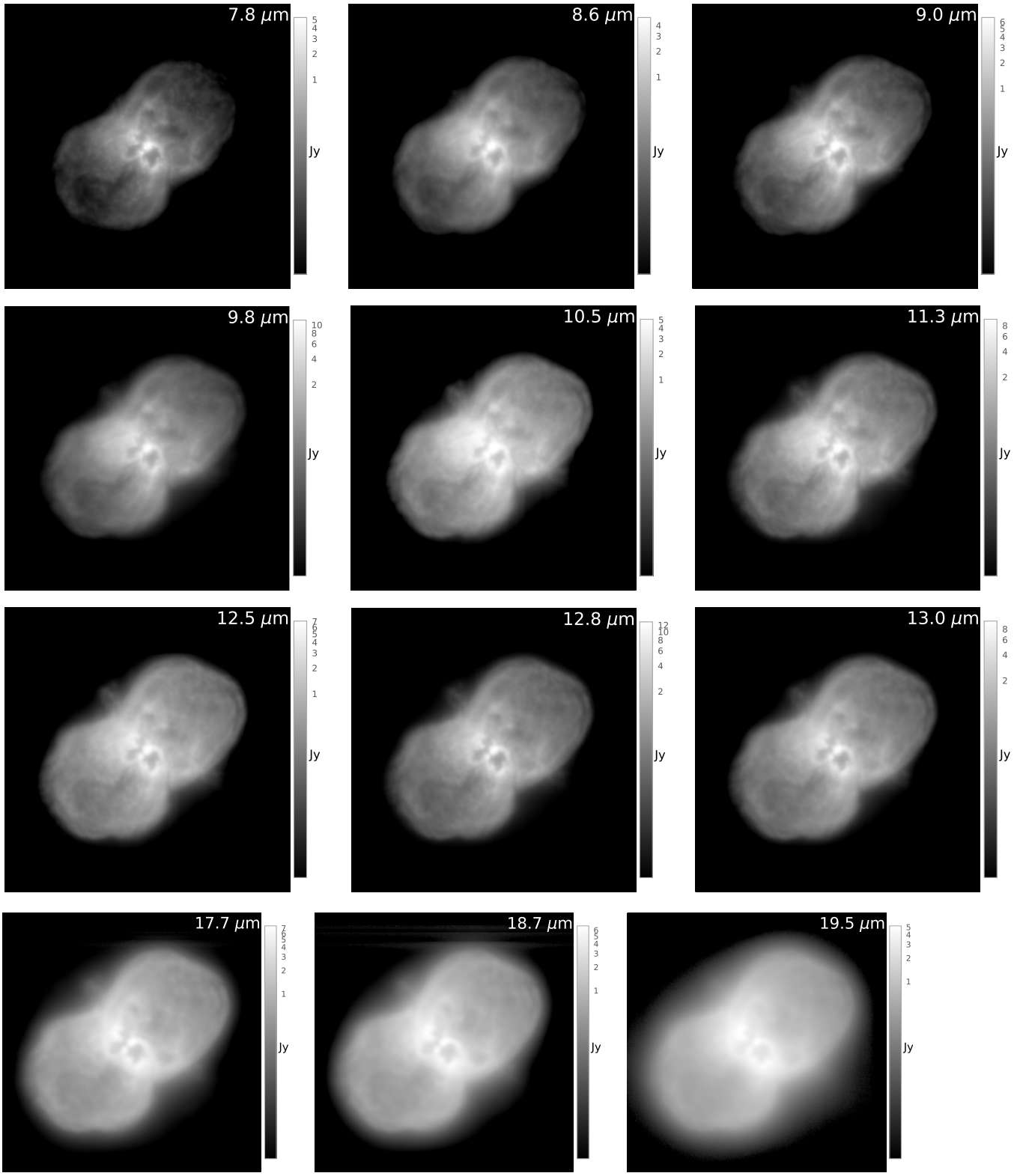

Fig. A.1. VISIR 2018 images of the Homunculus nebula around η Car. The flux density in Jy per detector pixel ($0.045'' \text{ pixel}^{-1}$) is shown on a logarithmic scale. The *N*-band images have a field of view of $25'' \times 25''$, and that of the *Q*-band images (last row) is $22.5'' \times 22.5''$.

Appendix B: Journal of VISIR and TIMMI2 observations

Table B.1. Journal of VISIR observations.

Date	MJD	Target	Filter	Wavelength (μm)	Image quality ($''$)	ESO PROG.ID
2005-01-23	53393.05	HD9138	PAH2	11.25	0.39	074.A-9016(A); PI: Lagage
2005-01-23	53393.10	HD59294	PAH2	11.25	0.36	074.A-9016(A)
2005-01-23	53393.18	HD30080	NEII	12.81	0.38	074.A-9016(A)
2005-01-23	53393.25	HD62902	NEII	12.81	0.38	074.A-9016(A)
2005-01-23	53393.37	η Car	NEII	12.81	0.38	074.A-9016(A)
2005-01-23	53393.37	η Car	PAH2	11.25	0.37	074.A-9016(A)
2018-04-28	58237.00	η Car	PAH1	8.59	0.23	0101.D-0077(A); PI: Mehner
2018-04-29	58237.00	η Car	SIV	10.49	0.27	0101.D-0077(A)
2018-04-29	58237.00	η Car	B12.4	12.47	0.31	0101.D-0077(A)
2018-04-29	58237.01	HD89682	PAH1	8.59	0.23	0101.D-0077(A)
2018-04-29	58237.02	HD89682	SIV	10.49	0.27	0101.D-0077(A)
2018-04-29	58237.02	HD89682	B12.4	12.47	0.31	0101.D-0077(A)
2018-05-11	58249.10	η Car	Q1	17.65	~0.50	0101.D-0077(A)
2018-05-11	58249.11	η Car	Q2	18.72	~0.50	0101.D-0077(A)
2018-05-11	58249.12	η Car	Q3	19.50	~0.50	0101.D-0077(A)
2018-05-11	58249.13	HD89682	Q1	17.65	~0.50	0101.D-0077(A)
2018-05-11	58249.13	HD89682	Q2	18.72	~0.50	0101.D-0077(A)
2018-05-11	58249.14	HD89682	Q3	19.50	~0.50	0101.D-0077(A)
2018-05-21	58259.97	η Car	J7.9	7.78	0.22	0101.D-0077(A)
2018-05-21	58259.98	η Car	SIV_1	9.82	0.31	0101.D-0077(A)
2018-05-21	58259.99	HD89682	J7.9	7.78	0.22	0101.D-0077(A)
2018-05-21	58260.00	HD89682	SIV_1	9.82	0.31	0101.D-0077(A)
2018-12-10	58462.31	η Car	ARIII	8.99	0.26	0101.D-0077(A)
2018-12-10	58462.31	η Car	PAH2	11.25	0.29	0101.D-0077(A)
2018-12-10	58462.32	η Car	NEII	12.81	0.33	0101.D-0077(A)
2018-12-10	58462.32	η Car	NEII_2	13.04	0.33	0101.D-0077(A)
2018-12-10	58462.33	HD89682	ARIII	8.99	0.26	0101.D-0077(A)
2018-12-10	58462.34	HD89682	PAH2	11.25	0.29	0101.D-0077(A)
2018-12-10	58462.34	HD89682	NEII	12.81	0.33	0101.D-0077(A)
2018-12-10	58462.35	HD89682	NEII_2	13.04	0.33	0101.D-0077(A)

Table B.2. Journal of TIMMI2 observations.

Date	MJD	Target	Filter	Wavelength (μm)	ESO PROG.ID
2003-01-26	52665.26	HD81797	N10.4	10.3	60.A-9126(C); Engineering run
2003-01-26	52665.26	HD81797	N11.9	11.6	60.A-9126(C)
2003-01-26	52665.26	HD81797	N10.4	10.3	60.A-9126(C)
2003-01-26	52665.27	HD81797	N11.9	11.6	60.A-9126(C)
2003-01-26	52665.27	HD81797	Q1	17.8	60.A-9126(C)
2003-01-26	52665.29	η Car	N7.9	7.9	60.A-9126(C)
2003-01-26	52665.30	η Car	N8.9	8.7	60.A-9126(C)
2003-01-26	52665.30	η Car	N10.4	10.3	60.A-9126(C)
2003-01-26	52665.3	η Car	N11.9	11.6	60.A-9126(C)
2003-01-26	52665.31	η Car	N12.9	12.3	60.A-9126(C)
2003-01-26	52665.32	η Car	[NeII]	12.8	60.A-9126(C)
2003-01-26	52665.32	η Car	Q1	17.8	60.A-9126(C)
2003-01-26	52665.33	η Car	N9.8	9.6	60.A-9126(C)
2003-01-26	52665.33	η Car	N9.8	9.6	60.A-9126(C)
2003-01-26	52665.34	HD81797	N7.9	7.9	60.A-9126(C)
2003-01-26	52665.35	HD81797	N8.9	8.7	60.A-9126(C)
2003-01-26	52665.35	HD81797	N9.8	9.6	60.A-9126(C)
2003-01-26	52665.35	HD81797	N10.4	10.3	60.A-9126(C)
2003-01-26	52665.35	HD81797	N11.9	11.6	60.A-9126(C)
2003-01-26	52665.35	HD81797	N12.9	12.3	60.A-9126(C)
2003-01-26	52665.36	HD81797	[NeII]	12.8	60.A-9126(C)
2003-01-26	52665.36	HD81797	Q1	17.8	60.A-9126(C)
2003-03-19	52717.45	HD156277	N10.4	10.3	60.A-9126(E); Engineering run
2003-03-19	52717.45	HD156277	[NeII]	12.8	60.A-9126(E)
2003-05-14	52773.07	HD123139	N10.4	10.3	60.A-9126(A); Engineering run
2003-05-14	52773.07	HD123139	N9.8	9.6	60.A-9126(A)
2003-05-14	52773.08	HD123139	N8.9	8.7	60.A-9126(A)

Table B.2. continued.

Date	MJD	Target	Filter	Wavelength (μm)	ESO PROG.ID
2003-05-14	52773.08	HD123139	N7.9	7.9	60.A-9126(A)
2003-05-14	52773.08	HD123139	N12.9	12.3	60.A-9126(A)
2003-05-14	52773.09	HD123139	[NeII]	12.8	60.A-9126(A)
2003-05-14	52773.10	HD123139	M	4.6	60.A-9126(A)
2003-05-14	52773.12	η Car	N7.9	7.9	60.A-9126(I); Engineering run
2003-05-14	52773.12	η Car	N7.9	7.9	60.A-9126(I)
2003-05-14	52773.12	η Car	N8.9	8.7	60.A-9126(I)
2003-05-14	52773.13	η Car	N10.4	10.3	60.A-9126(I)
2003-05-14	52773.13	η Car	N12.9	12.3	60.A-9126(I)
2003-05-14	52773.13	η Car	[NeII]	12.8	60.A-9126(I)
2003-05-14	52773.14	η Car	M	4.6	60.A-9126(I)
2003-05-14	52773.14	η Car	N7.9	7.9	60.A-9126(I)
2003-05-14	52773.15	η Car	N8.9	8.7	60.A-9126(I)
2003-05-14	52773.15	η Car	N7.9	7.9	60.A-9126(I)
2003-05-14	52773.15	η Car	N8.9	8.7	60.A-9126(I)
2003-05-14	52773.15	η Car	N9.8	9.6	60.A-9126(I)
2003-05-14	52773.15	η Car	N10.4	10.3	60.A-9126(I)
2003-05-14	52773.16	η Car	N12.9	12.3	60.A-9126(I)
2003-05-14	52773.16	η Car	[NeII]	12.8	60.A-9126(I)
2003-05-14	52773.16	η Car	M	4.6	60.A-9126(I)
2003-05-14	52773.96	HD108903	N7.9	7.9	69.D-0304(B); PI: Gehrz
2003-05-14	52773.97	HD108903	N8.9	8.7	69.D-0304(B)
2003-05-14	52773.97	HD108903	N9.8	9.6	69.D-0304(B)
2003-05-14	52773.97	HD108903	N10.4	10.3	69.D-0304(B)
2003-05-14	52773.97	HD108903	N11.9	11.6	69.D-0304(B)
2003-05-14	52773.97	HD108903	Q1	17.8	69.D-0304(B)
2003-05-14	52773.98	HD108903	M	4.6	69.D-0304(B)
2003-05-14	52773.98	η Car	N7.9	7.9	69.D-0304(B)
2003-05-14	52773.98	η Car	N8.9	8.7	69.D-0304(B)
2003-05-14	52773.99	η Car	N9.8	9.6	69.D-0304(B)
2003-05-14	52773.99	η Car	N10.4	10.3	69.D-0304(B)
2003-05-14	52773.99	η Car	N11.9	11.6	69.D-0304(B)
2003-05-14	52773.99	η Car	N11.9	11.6	69.D-0304(B)
2003-05-14	52774.00	η Car	N11.9	11.6	69.D-0304(B)
2003-05-15	52774.00	η Car	Q1	17.8	69.D-0304(B)
2003-05-15	52774.01	η Car	M	4.6	69.D-0304(B)
2003-05-15	52774.01	η Car	N8.9	8.7	69.D-0304(B)
2003-05-15	52774.01	η Car	N11.9	11.6	69.D-0304(B)
2003-05-15	52774.02	η Car	Q1	17.8	69.D-0304(B)
2003-05-15	52774.94	HD108903	N8.9	8.7	69.D-0304(B)
2003-05-15	52774.94	HD108903	N11.9	11.6	69.D-0304(B)
2003-05-15	52774.95	HD108903	Q1	17.8	69.D-0304(B)
2003-05-15	52774.95	HD108903	M	4.6	69.D-0304(B)
2003-05-15	52774.99	η Car	N7.9	7.9	69.D-0304(B)
2003-05-15	52774.99	η Car	N8.9	8.7	69.D-0304(B)
2003-05-15	52775.00	η Car	N9.8	9.6	69.D-0304(B)
2003-05-15	52775.00	η Car	N10.4	10.3	69.D-0304(B)
2003-05-15	52775.00	η Car	N11.9	11.6	69.D-0304(B)
2003-05-16	52775.00	η Car	N12.9	12.3	69.D-0304(B)
2003-05-16	52775.00	η Car	[NeII]	12.8	69.D-0304(B)
2003-05-16	52775.01	η Car	Q1	17.8	69.D-0304(B)
2003-05-16	52775.01	η Car	M	4.6	69.D-0304(B)
2003-05-16	52775.02	HD108903	N7.9	7.9	69.D-0304(B)
2003-05-16	52775.02	HD108903	N8.9	8.7	69.D-0304(B)
2003-05-16	52775.02	HD108903	N9.8	9.6	69.D-0304(B)
2003-05-16	52775.02	HD108903	N10.4	10.3	69.D-0304(B)
2003-05-16	52775.02	HD108903	N11.9	11.6	69.D-0304(B)
2003-05-16	52775.02	HD108903	N12.9	12.3	69.D-0304(B)
2003-05-16	52775.02	HD108903	[NeII]	12.8	69.D-0304(B)
2003-05-16	52775.03	HD108903	Q1	17.8	69.D-0304(B)
2003-05-16	52775.03	HD108903	M	4.6	69.D-0304(B)
2003-05-27	52786.94	HD110458	N7.9	7.9	71.D-0049(A); PI: Zijlstra
2003-05-27	52786.94	HD110458	N11.9	11.6	71.D-0049(A)
2003-05-27	52786.95	HD110458	N12.9	12.3	71.D-0049(A)
2003-05-27	52786.96	η Car	N7.9	7.9	71.D-0049(A)
2003-05-27	52786.97	η Car	N11.9	11.6	71.D-0049(A)
2003-05-27	52786.97	η Car	N12.9	12.3	71.D-0049(A)